NASA TM X-569

TECHNICAL MEMORANDUM

X-569

EFFECTS OF TRANSVERSE CENTER-OF-GRAVITY DISPLACEMENT, AFTERBODY GEOMETRY, AND FRONT-FACE CURVATURE ON THE AERODYNAMIC CHARACTERISTICS OF MERCURY-TYPE MODELS AT A MACH NUMBER OF 5.5

By Peter F. Intrieri

Ames Research Center
Moffett Field, Calif.

NATIONAL AERONAUTICS AND SPACE ADMINISTRATION

WASHINGTON

June 1961

1T

CONFIDENTIAL

NATIONAL AERONAUTICS AND SPACE ADMINISTRATION

TECHNICAL MEMORANDUM X-569

EFFECTS OF TRANSVERSE CENTER-OF-GRAVITY DISPLACEMENT, AFTERBODY GEOMETRY, AND FRONT-FACE CURVATURE ON THE AERODYNAMIC CHARACTERISTICS OF MERCURY-TYPE MODELS AT A MACH NUMBER OF 5.5*

By Peter F. Intrieri

SUMMARY

20540

Tests were made of Mercury-type models with a 26.5° half-angle conical afterbody in a pressurized ballistic range at a Mach number of 5.5 and a Reynolds number of 0.1×10^6. It was found that Newtonian theory accurately predicted the trim angles of attack obtained by transverse displacement of the center of gravity of models with a ratio of diameter to front face curvature of 1.0. The models were statically stable about a practical center-of-gravity location but were dynamically unstable. The afterbody apparently contributed to the static stability at large angles of attack. The drag and lift characteristics were well predicted by modified Newtonian theory. The effect of front-face curvature on the static stability was only qualitatively predicted by modified Newtonian theory.

INTRODUCTION

Studies of the entry of manned vehicles have shown that excessive deceleration due to atmospheric drag can be reduced and landing at a predetermined point can be greatly facilitated by the introduction of some lift on the vehicles. This discovery has created a need for investigation of controls capable of trimming configurations at angles of attack to produce the desired lift.

As part of a study program in this area, an investigation was conducted to determine the effectiveness of transverse center-of-gravity displacement in trimming a Mercury-type model at angles of attack. The basic configuration selected for testing was a vehicle with a front face

*Title, Unclassified

similar to the Project Mercury capsule, operated as a low L/D lifting body. (The Mercury has a face diameter to radius of curvature ratio, d/r_c, of 0.932. For the present models d/r_c was 1.0.) The afterbody, however, was modified. The original Mercury configuration developed a maximum L/D of about 3/8 at an angle of attack near -34° (ref. 1). At this angle of attack the afterbody was exposed to the free stream, was subjected to intense heating, and developed lift in opposition to that developed by the front face. For a lifting vehicle, an abbreviated afterbody was therefore indicated. It was considered that the afterbody, at the design lifting attitude, should either remain hidden behind the heat shield or at most, become parallel to the free-stream velocity vector. From the consideration that the front face could be approximated by a flat plate and that theory predicts a lift-drag ratio of 0.5 for a flat plate at an angle of attack of -26.5° (the angle of attack is defined to be zero when the plate is normal to the stream), the afterbody selected consisted of a 26.5° half-angle cone. Models of this configuration were used to determine the trim effectiveness of transverse center-of-gravity displacement. The aerodynamic characteristics of this configuration were compared with those of the Project Mercury capsule to show the effect of changing the afterbody geometry. One configuration with $d/r_c = 1/2$ and one with $d/r_c = 0$ were also tested to determine the effect of front-face curvature on the aerodynamic characteristics of the model.

The investigation was conducted in the Ames Pressurized Ballistic Range at a nominal Mach number of 5.5 and a nominal Reynolds number of 0.1 million, based on free-stream conditions and body diameter. The experimental results of this investigation, along with theoretical calculations, are presented and discussed herein.

SYMBOLS

A	reference area, maximum body cross-sectional area, sq ft
C_D	drag coefficient, $\frac{\text{total drag}}{q_\infty A}$
C_{l_α}	lift-curve slope, per radian
C_{m_α}	restoring-moment-curve slope, per radian
$C_{m_q}+C_{m_{\dot{\alpha}}}$	damping-in-pitch derivative, sec^{-1}
C_N	normal-force-curve slope, per radian
d	reference diameter, maximum body diameter, ft
I_Y	average transverse moment of inertia, mo^2, slug-ft^2

k	constant in equation (7)
$k_{1,2}$	constants in equation (8)
$K_{1,2,3}$	constants in equation (1), deg
$\frac{L}{D}$	lift-drag ratio
M	Mach number
m	mass of model, slugs
p	roll rate, radians/ft
q_∞	free-stream dynamic pressure, lb/sq ft
q	pitching rate, radians/sec
R	Reynolds number based on free-stream air properties and maximum diameter
r_c	radius of curvature of model front face, ft
X,Y,Z	earth-fixed axes; also displacements along these axes, ft
x_{cg}	axial distance from model maximum diameter station to center of gravity, ft
z_{cg}	transverse distance from model axis to center of gravity, ft
α	angle of attack in earth-fixed axes (angle between model axis and resultant wind direction projected onto the vertical XZ plane), deg
α_r	resultant angle of attack, $\sqrt{\alpha^2+\beta^2}$, deg
α_{RMS}	root-mean-square resultant angle of attack, $\sqrt{\frac{\int_0^x \alpha_r^2}{x}}$, deg
α_{trim}	resultant angle of attack for trim, deg
β	angle of sideslip in earth-fixed axes (angle between model axis and resultant wind direction projected onto the horizontal XY plane), deg

δ angle between model axis and a line from the center of curvature through the center of gravity (see sketch in fig. 5), deg

η_1, η_2 damping exponents in equation (1), ft^{-1}

λ wavelength of pitching oscillation, ft/cycle

ξ dynamic stability parameter, $C_D - C_{L_\alpha} + (C_{m_q} + C_{m_{\dot{\alpha}}})\left(\frac{d}{\sigma}\right)^2$

ρ air density, slugs/cu ft

σ transverse radius of gyration, ft

ϑ, ψ attitude coordinates of the model relative to earth-fixed axes, deg

ω_1, ω_2 rates of rotation of complex vectors which generate the model pitching motion, radians/ft

$(\dot{})$ first derivative with respect to time

$(')$ first derivative with respect to distance

A 5 3 7

Subscripts

Except where otherwise defined, the following subscripts apply:

cg center of gravity

i initial conditions

∞ free-stream conditions

DESCRIPTION OF TESTS

Models and Sabots

Sketches of the models showing pertinent nominal dimensions are presented in figure 1. A sketch of the Project Mercury capsule is presented superimposed on the sketch of the present $d/r_c = 1$ configuration to show the difference in afterbody geometry. The models were machined from phosphor bronze and were homogeneous, resulting in the center-of-gravity positions shown. Several of the basic models ($d/r_c = 1$)

were internally ballasted to effect transverse center-of-gravity displacements, z_{cg}/d, of about 0.013 and 0.032, to trim the models at predicted nominal angles of attack of 8° and 20°, respectively. The position of the center-of-gravity for the various models was measured to within 0.0005 inch. The dimensions of the models for each configuration deviated only slightly from those shown in figure 1. The measured physical characteristics of each model are listed in table I.

Photographs of the basic model and sabots are presented in figure 2. The straight sabots (fig. 2(a)) were used to launch the homogeneous models at zero angle of attack, and the canted sabots (fig. 2(b)) were used to launch the models with the displaced centers of gravity. The sabots were made of Lexan plastic and split in two pieces, as shown. The models were held in the correct attitude in the sabots by a small peened over portion of the sabot lip.

Test Technique and Test Conditions

The models were tested in free flight by launching them from a caliber 50 smooth-bore gun at a nominal velocity of 6200 feet per second, corresponding to a nominal Mach number of 5.5, into the test section of the Ames Pressurized Ballistic Range. Some of the models - those with $z_{cg} \neq 0$ - had trim lift coefficients as large as 0.4. This created a problem in testing, since they tended to fly a curved trajectory and thus to fly out of the instrumented region of the range. As a means of controlling the amount of path curvature, the tests were conducted at reduced static pressure. The test-section static pressure was adjusted to 1 psia, which corresponds to a nominal Reynolds number of 0.1 million based on free-stream conditions and model diameter. Table II lists the average values of Mach number and Reynolds number for each flight.

The trajectory of the model through the test section was recorded over a 130-foot length in 17 shadowgraph stations located at various intervals along the test section. Each station recorded side- and plan-view shadowgraphs along with reference wires from which X, Y, Z, θ, and ψ coordinates could be read; the linear coordinates within 0.005 inch, and angles within 0.25°. The orientation angles θ and ψ were read relative to earth-fixed axes. Corrections were made for the angle between the resultant wind direction and the earth-fixed axes to give values of α and β. Time of model flight between stations was recorded in a precision chronograph to within 5/8 microsecond. Typical shadowgraph pictures of the model in flight are presented in figures 3(a) and (b). These pictures show the presence of laminar-boundary-layer flow back to the minimum diameter station of the wake and fully separated flow over the afterbody at small angles of attack.

REDUCTION OF DATA

Stability derivatives and trim angle of attack were obtained from analysis of the pitching and yawing motions of the models by fitting the following equation to the measurements of α and β of each flight.

$$\beta + i\alpha = K_1 e^{(\eta_1 + i\omega_1)X} + K_2 e^{(\eta_2 - i\omega_2)X} + K_3 e^{ipX} \qquad (1)$$

Equation (1) is the solution of the linear differential equation of motion as given in reference 2. Some of the basic assumptions used in the development of this equation are: axially symmetric configuration, linear force and moment system, small angular displacements, and small angles of trim. Equation (1) was programmed for machine computation to select optimum values of the constants by an iterative process of differential corrections. The resultant angle of attack for trim is given by the value of K_3 in equation (1).

A 5 3 7

The static stability derivative, C_{m_α}, was computed from the wave length of oscillation by means of the following relation:

$$C_{m_\alpha} = \frac{8\pi^2 I_Y}{\lambda^2 \rho A d} \qquad (2)$$

where

$$\lambda = \frac{2\pi}{\omega_1 \omega_2} \qquad (3)$$

The dynamic stability parameter, ξ, was determined from the constants η_1 and η_2 by means of the relation

$$\eta_1 + \eta_2 = \frac{\rho A}{2m} \xi \qquad (4)$$

where

$$\xi = C_D - C_{L_\alpha} + (C_{m_q} + C_{m_{\dot{\alpha}}})\left(\frac{d}{\sigma}\right)^2 \qquad (5)$$

The lift-curve slope was obtained from analysis of the swerving motion of the models by fitting the following equation to the measurements of Z and Y of each flight.

$$-Y + iZ = (-Y + iZ)_1 + (-Y + iZ)'_1 X + \frac{\rho A}{2m}\left[C_{L_\alpha}\int_0^X\int_0^X(\beta + i\alpha)dX\,dX\right.$$

$$\left. + (-C_{Y_o} + iC_{L_o})\frac{1 + ipX - e^{iX}}{p^2}\right] \qquad (6)$$

where $(-C_{Y_o} + iC_{L_o})$ represents a constant transverse force fixed to the model at zero angle of attack. Equation (6) is the solution of the linear differential equation for the swerving motion presented in reference 2. Application of this equation is dependent on a prior evaluation of the constants present in equation (1). Equation (6) was adapted for machine computation employing a least-squares fit to the observed swerving motion to optimize the calculated constants.

The analysis just described is based upon the necessary assumption that the aerodynamic coefficients vary linearly with angle of attack. It is not possible at the present time to obtain solutions to the basic differential equations of motion if such an assumption is not made. References 3 and 4 describe methods of analysis which, while avoiding this limitation to linear aerodynamics, are forced to impose restrictions of zero roll and/or zero trim angle, preventing the application of these methods to the data of this report. Theoretical calculations indicate that the aerodynamic coefficients of the models used in the present investigation are nonlinear. Therefore, it must be realized that the experimental coefficients presented in this analysis are the aerodynamic coefficients of an equivalent linear system that provides the best possible fit to the motion actually experienced by the model.

Illustrations of the types of motions encountered in the present tests, as viewed in the $\alpha - \beta$ plane, are shown in figure 4. Since the models are aerodynamically symmetric, the angular displacement of the model, at any instant, can be represented also by the resultant angle of attack α_r, whose orthogonal components are the angles α and β. Figures 4(a), (b), and (c) represent the motions obtained by three basic models ($d/r_c = 1$) trimmed at nominal resultant angles of attack of 0°, 8°, and 20°, respectively. It can be seen that, in general, the data show precessing elliptical motions, and that the angle range through which the models oscillate is quite large and differs for each flight. The curves shown in figure 4 were obtained by fitting equation (1) to the experimental data. The fitted curves agreed closely with the measured angles - in fact, the agreement was within the measuring accuracy.

It is important to mention that the machine-programmed iterative solution of equation (1), used to obtain values of the stability derivatives and trim angles of attack, did not converge for two of the three flights obtained for the basic model trimmed at a nominal angle of attack of 20° (flights 226 and 228). In the third, flight number 231,

the process did converge, although extremely slowly (36 iterations were required for convergence of this run as compared to about 4 or 5 for the other runs). Although the analysis was divergent for flight numbers 226 and 228, values of C_{m_α}, ξ, and α_{trim} were obtained, based on initial values of the constants which were determined by a preliminary graphical analysis of the motion and used as input values for the machine program. The initial values resulted in a good fit to the observed angular motion of the two flights and so were used. Although the divergence of the analysis for these two flights is not considered conclusive evidence, it is believed indicative that the analysis, which assumes small angles of trim, breaks down when these angles approach 20°.

The reduction of drag coefficient from the time-distance data was based on the procedure described in reference 5, which assumes a constant drag coefficient. A procedure applicable to cases where the drag coefficient varies with angle of attack is presented in reference 6. It is shown in reference 6 that if the drag coefficient varies with the square of the local resultant angle of attack, according to the relation

$$C_D = C_{D_0} + k\alpha_r^2 \tag{7}$$

the drag coefficient obtained by the method of reference 5, under certain additional constraints, is the drag coefficient that would be obtained at a resultant angle of attack equal to the root-mean-square resultant angle of attack. For the present investigation, the theoretical variation of C_D with α dictated the addition of a fourth-power term to equation (7). The equation used in the present analysis takes the form

$$C_D = C_{D_0} + k_1\alpha_r^2 + k_2\alpha_r^4 \tag{8}$$

It can be shown, in a manner similar to that used in reference 6, that the effective drag coefficient obtained from the present data by the method of reference 5, under the same restraints, is also the drag coefficient that would be obtained at a resultant angle of attack equal to the α_{RMS} of the flight. To simplify correlation of the data it was assumed that the right-hand side of equation (8) was a perfect square. Hence, the expression for drag coefficient becomes

$$\sqrt{C_D} = \sqrt{C_{D_0}} - \sqrt{k_2}\alpha_r^2 \tag{9}$$

and

$$k_1 = -2\sqrt{C_{D_0}}\sqrt{k_2} \tag{10}$$

Although arbitrary in form, equation (9) showed excellent correlation with the modified Newtonian theory. An experimental variation of C_D with α was obtained by using a least-squares procedure to fit equation (9) to the experimental values of $\sqrt{C_D}$ and $(\alpha_{RMS})^2$.

RESULTS AND DISCUSSION

A total of 13 flights were made for analysis of lift, drag, aerodynamic stability, and trim angle of attack. Eleven flights were made of the basic ($d/r_c = 1$) configuration and one flight each of configurations with ratios of diameter to radius of curvature of 1/2 and 0. Experimental values of α_{trim}, C_{m_α}, C_{l_α}, ξ, and C_D are summarized in table II. Theoretical estimates of the aerodynamic coefficients were made using Newtonian impact theory (ref. 7), modified by use of a stagnation pressure coefficient of 1.8.

It should be re-emphasized that with the exception of drag coefficient, the experimentally derived coefficients are those of an equivalent linear system that most nearly matches the recorded motion. If the actual coefficients are linear, or nearly so, with angle of attack, the analysis is straightforward and comparison can be made with theory. If, on the other hand, the actual coefficients are nonlinear with angle of attack and the angular excursions are large, no justification exists for direct comparison of theory with the equivalent linear coefficients determined from the experiments. Direct comparison, with theory, of the effective drag coefficient as determined for the present tests is justified.

Trim Effectiveness of Transverse Center-of-Gravity Displacement

The effectiveness of transverse center-of-gravity displacement in trimming the basic model at angles of attack is presented in figure 5. Transverse displacement of the center of gravity is given in terms of the angle δ, which is the angle between the model's x axis and the line from the center of curvature of the front face through the measured center of gravity (see sketch in fig. 5). The angle δ is plotted as a function of the measured resultant angle of attack for trim. The dashed curve represents the variation of δ with α_{trim} as estimated by Newtonian theory. The experimental values are in excellent agreement with those predicted by theory. The afterbody, which is not considered in the theory, apparently has little effect on the trim characteristics of this configuration at angles of trim up to 20°. The effect of the afterbody at higher angles of attack may, however, be significant. If this is the case then to trim at these higher angles may require

transverse center-of-gravity displacements in excess of those indicated by theory. With the center of gravity axially located 0.20 diameter aft of the maximum diameter, this configuration can be trimmed at angles of attack as high as 20° with a z_{cg}/d displacement of about 3 percent. This transverse displacement required for trim can be reduced by further aft positioning of the center of gravity.

Effect of Afterbody Geometry on the Aerodynamic Characteristics

The aerodynamic characteristics of the basic model ($d/r_c = 1$) compared with those of the Project Mercury capsule, obtained from similar free-flight tests reported in reference 8, are presented in figure 6. The data are plotted as a function of the root-mean-square resultant angle of attack, α_{RMS}, which may be regarded as an approximation to the effective angle of attack. The moment data of reference 8 were corrected to the center-of-gravity position of the present tests using the value of C_{N_α} at zero angle of attack estimated by Newtonian theory. This procedure should be satisfactory because the required correction was very small.

A 5 3 7

The experimental values of the static stability derivative, C_{m_α}, presented in figure 6(a), show that although both configurations are statically stable, the stability of the present configuration is about half that of the Mercury capsule in the low-angle-of-attack region for the present center-of-gravity position. Since the front faces of these configurations are very similar (the difference in d/r_c of the faces would account for only 2 percent of the difference in stability), it follows that the large difference in stability must be due to the different Mach numbers and Reynolds numbers of the tests and/or the different afterbody geometry of the configurations. It should be noted that the data of reference 8 were obtained at Mach numbers that were both higher and lower than the Mach number of the present tests, but showed very little effect of Mach number at low angles of attack. Furthermore, comparison of the static stability results of the present tests with unpublished data obtained at approximately the same Mach number, but at a much higher Reynolds number ($R_\infty \approx 3\times10^6$), indicates little effect of Reynolds number on the static stability of the present configuration at low angles of attack. Therefore, the large difference in stability must be due primarily to the different afterbody geometry of the configurations. For the present configuration in the low-angle-of-attack range, the measured values of C_{m_α} are about 15 percent below the value estimated by Newtonian theory at zero angle of attack indicated by the tick on the scale. Since the Newtonian theory gives only the stability of the front face and since any effect of the afterbody would be expected to increase the stability, it would appear that there is very little contribution to the stability by the afterbody of the present

configuration at low angles of attack. In contrast to the above comparison, the measured C_{m_α} values for the Mercury capsule are almost twice the value predicted by Newtonian theory and show the strong contribution to the stability by the afterbody of this configuration.

The Newtonian theory indicates that the stability of the present configuration decreases with increasing angle of attack. The measured data show that the stability does not change with angle of attack; therefore, for the same reasons given above, it appears that the afterbody is contributing to the stability as the angle of attack is increased. Although a fair amount of scatter is apparent in the experimental data for the Mercury capsule at a Mach number of 3.0, a similar independence of C_{m_α} with angle of attack is suggested. The Mercury-capsule data at a Mach number of 9, on the other hand, show a definite dependence upon angle of attack. It is interesting to note that for the Mercury-capsule tests at a Mach number of 3 and the present tests, the flow was fully separated over the afterbody at small angles of attack. For the Mercury-capsule tests at a Mach number of 9, on the other hand, the flow was such that a local laminar separation bubble occurred at the beginning of the afterbody with the flow impinging two-thirds of the cone length back on the afterbody, again indicating the importance of afterbody flow on the static stability of these configurations.

The dynamic stability parameters, ξ, of the two configurations are compared in figure 6(b). The values presented show appreciable scatter due to the relatively short trajectories used for analysis; however, certain meaningful results can be deduced. The results show that both configurations are dynamically unstable. The experimental values of ξ, obtained for the present configuration, vary from 1 to 3 for the angle-of-attack range presented, and are approximately equivalent to a divergence of less than 5 percent per cycle. The values of ξ, presented for the Mercury capsule (ref. 8), range from about 1 to 5, and show a strong dependence of this parameter on Mach number and angle of attack. As can be seen, the dynamic instability becomes less severe with increasing Mach number and increasing angle of attack. The values of ξ, measured for the present configuration at low angles of attack, fall between the values presented for the Mercury capsule at the two Mach numbers. It is important to mention that the present test data presented in figure 6(b) were obtained from tests of smooth-faced models which had separated flow over the afterbody as is shown in figure 3. It was reported in reference 8 that for a Mercury capsule with a roughened front face, the turbulent flow caused by the roughness resulted in a completely attached turbulent boundary layer on the afterbody which adversely affected the dynamic stability. A value of ξ of about 14 was measured for this flight.

The measured values of lift-curve slope obtained for the present $d/r_c = 1$ configuration are presented in figure 6(c). Comparison of these data with data for the Mercury capsule is not possible, since the lift characteristics of the latter were not determined in reference 8. The models exhibit a negative lift-curve slope for the angle-of-attack range presented, a characteristic associated with extremely blunt bodies. A mean fairing through the data would give a value of C_{L_α} at zero angle of attack, about 7 percent higher than the theoretical value indicated by the tick on the scale. A nonlinearity of C_{L_α} with angle of attack is predicted by Newtonian theory and is evident in the experimental data which show a decrease in the value of C_{L_α} as the α_{RMS} is increased.

The experimental values of drag coefficient presented in figure 6(d) show that the drag of the present configuration is slightly less than that obtained for the Mercury capsule, and about 4 percent less than the values predicted by theory in the low angle-of-attack range. The difference in drag coefficient between the present configuration and the Mercury capsule can be accounted for by the theoretical change in C_D due to the difference in front-face curvature of these configurations; therefore, it can be concluded that the afterbody has no effect on these data. The measured values of C_D are less than theory, probably due to a relieving of the pressure forces on the outer edge of the front face and a finite pressure acting on the afterbody, effects not considered in the theory. The variation of C_D with angle of attack given by theory and experiment is in good agreement.

Effect of Front-Face Curvature on the Aerodynamic Characteristics

The effect of front-face curvature on the static stability is shown in figure 7, where C_{m_α} is plotted as a function of diameter-to-radius-of-curvature ratio (d/r_c). It should be noted that the measured values of C_{m_α} presented in this figure were obtained at some angle of attack other than zero; and hence, are not strictly comparable to the estimated values computed for zero angle of attack. However, since the measured values of C_{m_α} for the $d/r_c = 1$ configuration, presented in figure 6(a), were independent of angle of attack, it is reasonable to assume that the measured values of C_{m_α} for the $d/r_c = 1/2$ and $d/r_c = 0$ configurations are also independent of angle of attack. Therefore, direct comparison of the measured values with the estimated values is believed acceptable in this case. The experimental results show that the three configurations are statically stable and that the stability increases with increasing curvature of the front face, being about 60 percent greater for the $d/r_c = 1$ configuration than for the flat-faced model. Although Newtonian theory predicts neutral stability for the flat-faced model, it is believed that a moving center of pressure on the front face provides

the stability observed experimentally. Furthermore, the theory underestimates the stability of the $d/r_c = 1/2$ configuration by about 10 percent and, as discussed previously in relation to the data presented in figure 6(a), overestimates the stability of the $d/r_c = 1$ configuration by about 15 percent. Thus, it can be concluded that the stability of these configurations improves with increased face curvature, and that Newtonian theory is reliable only for indicating the qualitative trends and not for giving the detailed variation.

The measured values of ξ and C_{L_α}, obtained for one configuration of $d/r_c = 1/2$ and one configuration of $d/r_c = 0$, are listed in table II. The variation in the experimental values of these coefficients obtained for the $d/r_c = 1$ configuration indicates that it would be unreasonable to attempt any correlation regarding the effect of face curvature on these parameters on the basis of a single test point. However, it appears that there is no strong dependence of ξ on face curvature.

The effect of front-face curvature on the drag coefficient is shown in figure 8. The results show that at a particular angle of attack, the drag coefficient increases with decreasing curvature of the front face. The pattern of agreement between the theory and the measured data shown for the $d/r_c = 1$ configuration, originally presented in figure 6(d), is apparently maintained between the measured values of C_D obtained for the $d/r_c = 1/2$ and $d/r_c = 0$ configurations and the corresponding theoretical values.

The L/D values for the three faces were not determined experimentally, because of the difficulty in defining the lift-curve slope as a function of angle of attack. However, the good agreement between theory and the measured values of C_{L_α} and C_D as a function of angle of attack (figs. 6(c) and (d)) suggests that the theory can be used to gain some insight into the relative values of L/D for the three faces. Therefore, values of L/D were calculated using the modified Newtonian theory and are shown in figure 9. These results indicate that the angle of attack required to achieve a given value of L/D is reduced as the face curvature is decreased. The importance of obtaining the desired L/D at a small angle of attack is twofold: First, the smaller the design angle of attack, the larger the afterbody volume may be without exposing the afterbody to the free stream. Second, the smaller the design angle of attack, the smaller the required control moment for trim. It is indicated from figure 9 that with a face curvature of $d/r_c = 1/2$ the angle of attack required to achieve a given value of L/D approaches a minimum (that for a flat face) and, hence, for the above reasons this face curvature may prove desirable. Figure 7 shows that the stability for the $d/r_c = 1/2$ configuration is smaller than the stability for the $d/r_c = 1$ configuration, which again implies that a smaller control

moment would be required for trim. Therefore, it appears that in future work on configurations of this type, attention should be given to face curvatures of $d/r_c \approx 1/2$ and afterbody angles of about 30°.

SUMMARY OF RESULTS

Ballistic range tests at a Mach number of 5.5 and a Reynolds number of 0.1×10^6 have been made of Mercury-type models with a 26.5° half-angle conical afterbody. Results of this investigation can be summarized as follows.

Models with a diameter-to-front-face-curvature ratio (d/r_c) of 1.0 were trimmed at angles of attack as high as 20° with a transverse center-of-gravity displacement, z_{cg}/d, of about 3 percent, with the center of gravity axially located 0.20 diameter aft of the maximum diameter. The trim angles of attack obtained experimentally were in excellent agreement with those predicted by Newtonian theory.

The models were statically stable for the center-of-gravity location tested. The static stability of the present $d/r_c = 1$ configuration was about half that of the Project Mercury capsule; this difference in stability was found to be due to the different afterbody geometry of the configurations. The afterbody of the present configuration had little effect on the stability at low angles of attack, but contributed to the stability as the angle of attack was increased.

The models were all dynamically unstable a small amount, approximately equivalent, for the present test conditions, to a divergence of less than 5 percent per cycle.

The drag and lift characteristics were well predicted by modified Newtonian theory.

Decreasing the curvature of the front face from a d/r_c of 1 to 0 decreased the static stability of the models by about 40 percent and increased the drag coefficient by about 15 percent. The effect of front-face curvature on the drag characteristics of the configurations was well predicted by modified Newtonian theory; its effect on static stability was only qualitatively indicated.

Ames Research Center
National Aeronautics and Space Administration
Moffett Field, Calif., April 20, 1961

REFERENCES

1. Brown, Steve W., and Moseley, William C., Jr: Summary of Wind-Tunnel Investigations of the Static Longitudinal Stability Characteristics of the Production Mercury Configurations at Mach Numbers from 0.05 to 20. NASA TM X-491, 1961.

2. Nicolaides, John D.: On the Free Flight Motion of Missiles Having Slight Configurational Asymmetries. BRL Rep. 858, Aberbeen Proving Ground, 1953.

3. Kirk, Donn B.: A Method for Obtaining the Nonlinear Aerodynamic Stability Characteristics of Bodies of Revolution from Free-Flight Tests. NASA TN D-780, 1961.

4. Rasmussen, Maurice L.: Determination of Nonlinear Pitching-Moment Characteristics of Axially Symmetric Models from Free-Flight Data. NASA TN D-144, 1960.

5. Seiff, Alvin: A New Method for Computing Drag Coefficients from Ballistic Range Data. Jour. Aero. Sci., vol. 25, no. 2, Feb. 1958, pp. 133-134.

6. Seiff, Alvin, and Wilkins, Max E.: Experimental Investigation of a Hypersonic Glider Configuration at a Mach Number of 6 and at Full-Scale Reynolds Numbers. NASA TN D-341, 1961.

7. Grimminger, G., Williams, E. P., and Young, G. B. W.: Lift on Inclined Bodies of Revolution in Hypersonic Flow. Jour. Aero. Sci., vol. 17, no. 11, Nov. 1950, pp. 675-690.

8. Sommer, Simon C., Short, Barbara J., and Compton, Dale L: Free-Flight Measurements of Static and Dynamic Stability of Models of the Project Mercury Re-entry Capsule at Mach Numbers 3 and 9.5. NASA TM X-373, 1960.

TABLE I.- PHYSICAL CHARACTERISTICS OF MODELS

Flight number	$\frac{d}{r_c}$	d, in.	$\frac{x_{cg}}{d}$	$\frac{z_{cg}}{d}$	δ, deg	$m \times 10^3$, slug	$I_Y \times 10^7$, slug-ft^2
144	1	0.449	0.199	0	0	0.2917	0.338
166	1	.450	.198	0	0	.2919	.337
191	1	.450	.200	0	0	.2934	.337
171	1	.449	.201	0.0147	1.26	.3093	.345
172	1	.450	.201	.0117	1.00	.3136	.356
173	1	.449	.201	.0122	1.05	.3091	.346
203	1	.449	.197	.0134	1.14	.3108	.343
224	1	.450	.200	.0125	1.07	.3123	.342
226	1	.450	.198	.0317	2.72	.3181	.340
228	1	.450	.199	.0335	2.88	.3171	.338
231	1	.449	.196	.0316	2.70	.3157	.334
162	1/2	.449	.224	0	0	.2645	.293
165	0	.451	.251	0	0	.2453	.258

A 5 3 7

TABLE II.- TEST CONDITIONS AND FINAL DATA

Flight number	M	$R_\infty \times 10^{-6}$	α_{RMS}, deg	α_{trim}, deg	C_{m_α}	ξ	C_{L_α}	C_D
144	5.40	0.17	7.00	0	-0.128	1.42	-1.409	1.498
166	5.50	.13	5.14	0	-.127	1.74	-1.245	1.500
191	5.40	.09	23.80	0	-.124	.83	-.875	1.247
171	5.48	.08	11.88	8.1	-.138	2.24	-1.037	1.444
172	5.59	.10	14.94	7.8	-.135	.93	-1.162	1.388
173	5.58	.13	20.99	9.6	-.119	1.94	-.845	1.285
203	5.51	.09	20.18	8.8	-.133	1.93	-.993	1.367
224	5.44	.09	14.73	7.9	-.139	.96	-1.116	1.415
226	5.63	.10	20.99	19.0	-.139	2.23	---	1.327
228	5.43	.09	23.46	20.0	-.129	2.82	---	1.251
231	5.58	.10	22.36	20.5	-.133	2.75	-.834	1.307
162	5.43	.13	9.25	0	-.109	2.57	-1.368	1.644
165	5.31	.13	17.06	0	-.080	1.01	-1.484	1.566

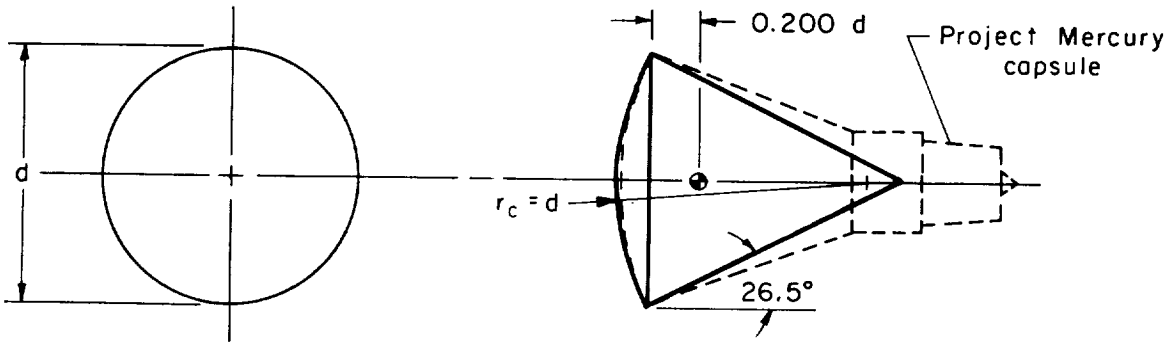

(a) $\frac{d}{r_c} = 1$ model.

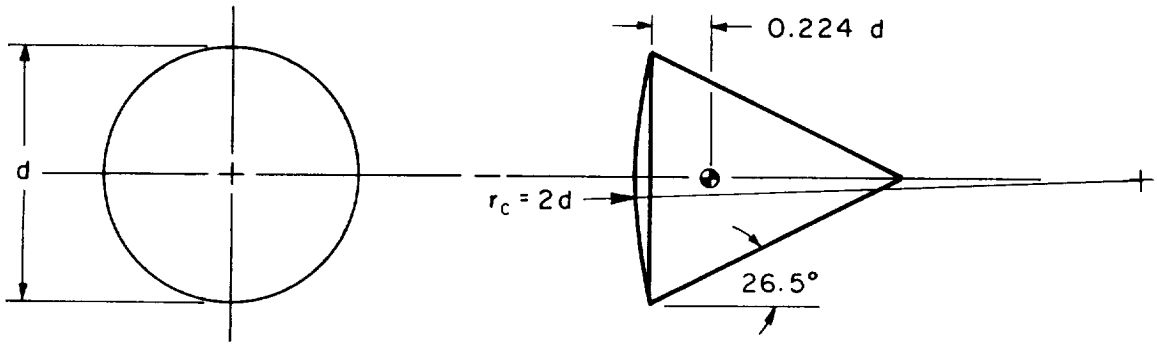

(b) $\frac{d}{r_c} = \frac{1}{2}$ model.

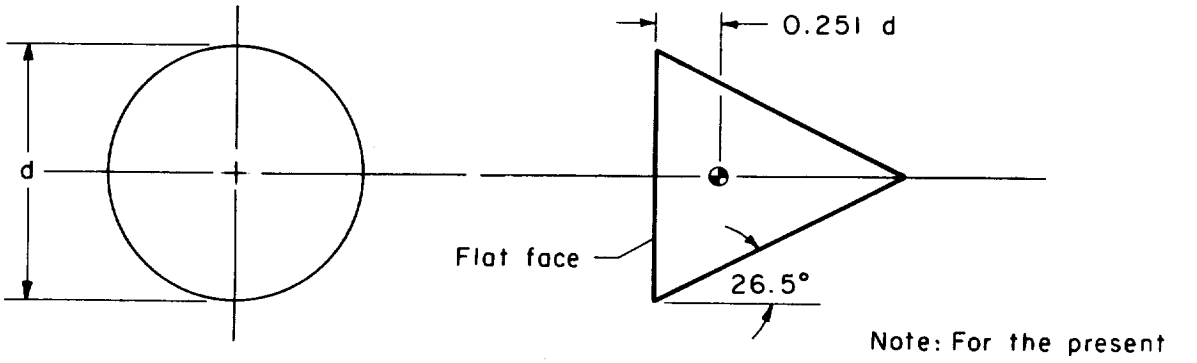

(c) $\frac{d}{r_c} = 0$ model.

Figure 1.- Sketches of the models showing nominal dimensions.

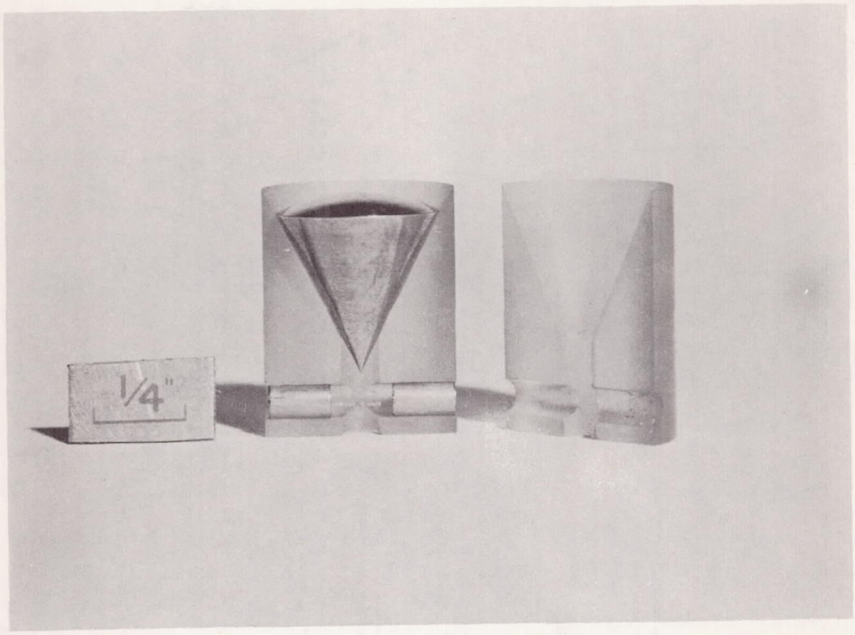

A-27706

(a) Model with straight sabot.

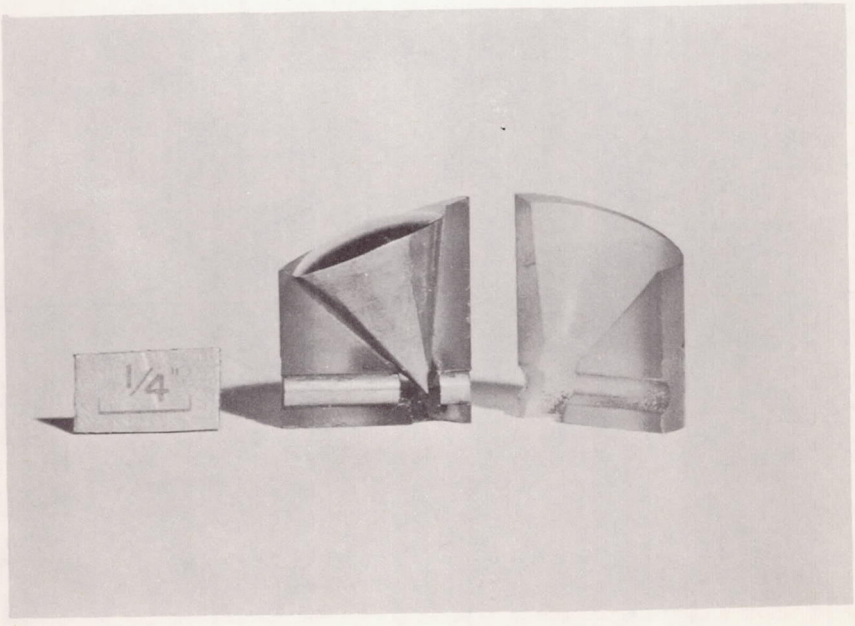

A-27707

(b) Model with canted sabot.

Figure 2.- Photographs of basic models and sabots.

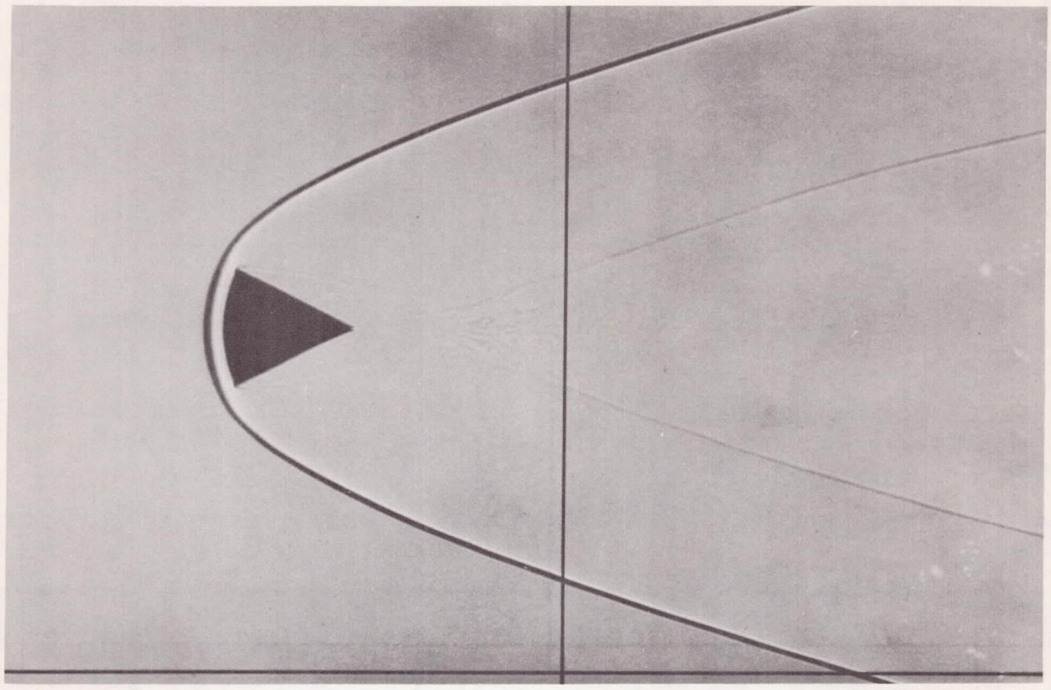

A-27708

(a) $\alpha = 0.64^{\circ}$ ($\beta = -0.31^{\circ}$)

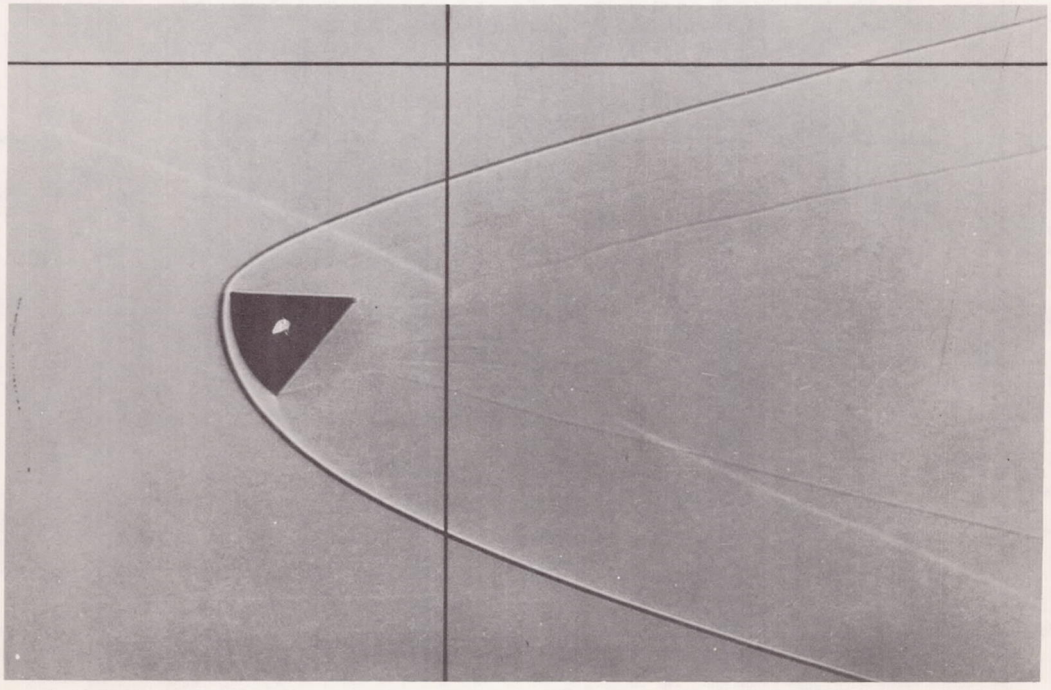

A-27709

(b) $\alpha = -24.85^{\circ}$ ($\beta = -3.93^{\circ}$)

Figure 3.- Typical shadowgraphs of basic model; M = 5.5; R = 0.1×10^{6}.

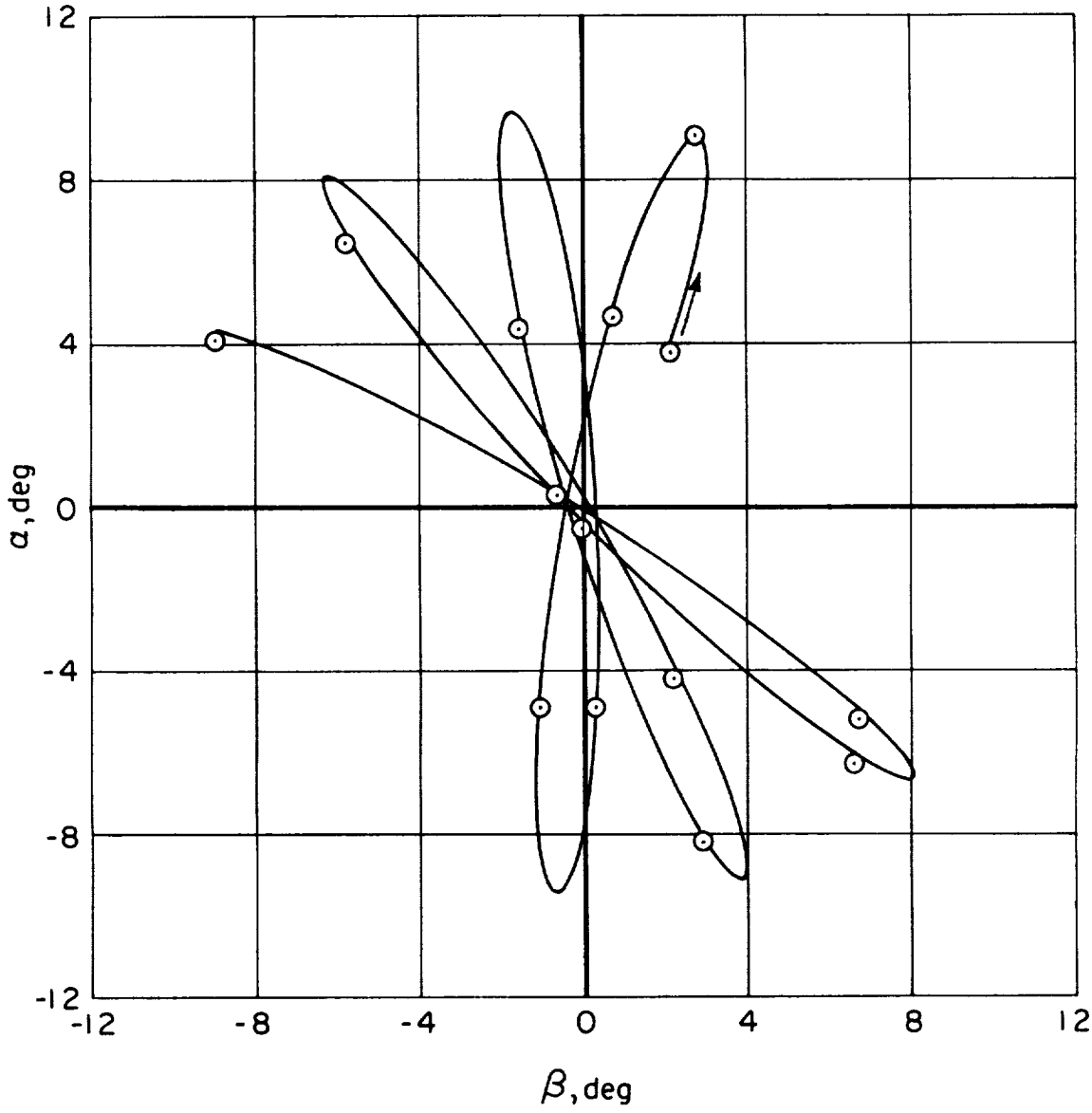

(a) Flight number 144; $\alpha_{trim} \approx 0^{\circ}$.

Figure 4.- Typical pitching and yawing motions; $\frac{d}{r_c} = 1$.

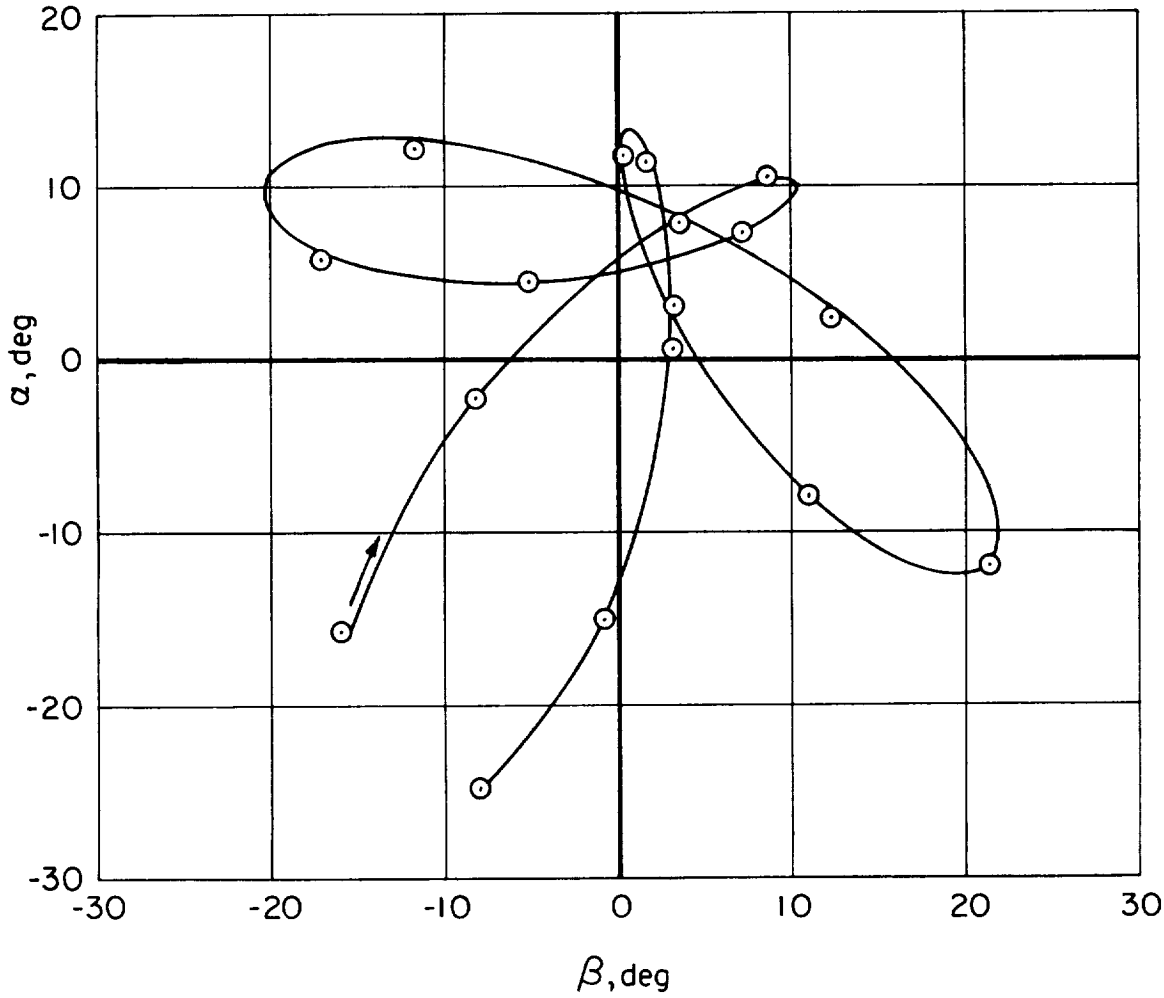

(b) Flight number 172; $\alpha_{trim} \approx 8^{\circ}$.

Figure 4.- Continued.

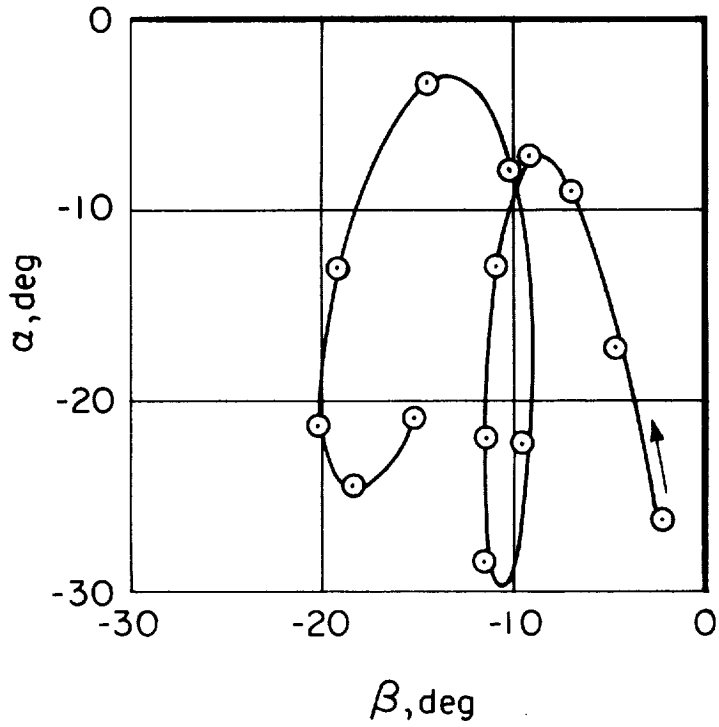

(c) Flight number 231; $\alpha_{trim} \approx 20^{\circ}$.

Figure 4.- Concluded.

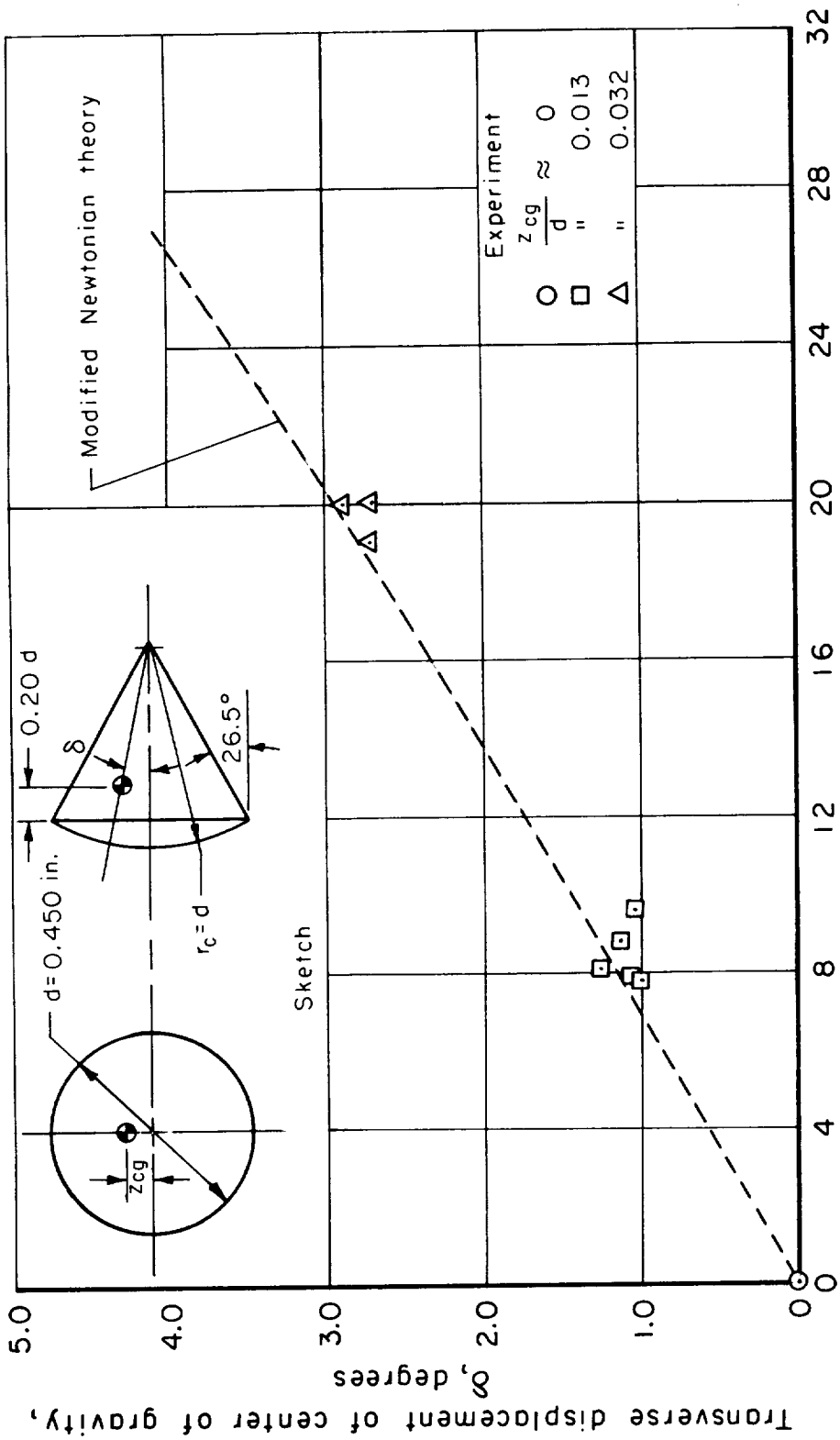

Figure 5.- Trim effectiveness of transverse center-of-gravity displacement; $\frac{d}{r_c} = 1$.

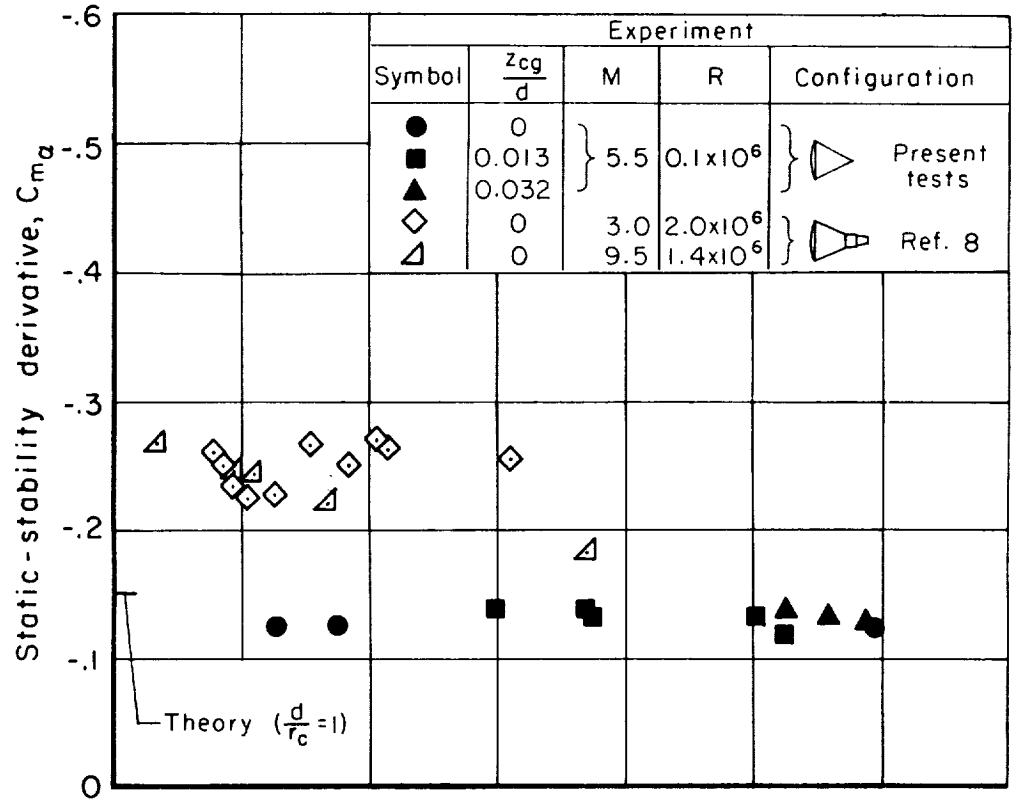

(a) Static stability.

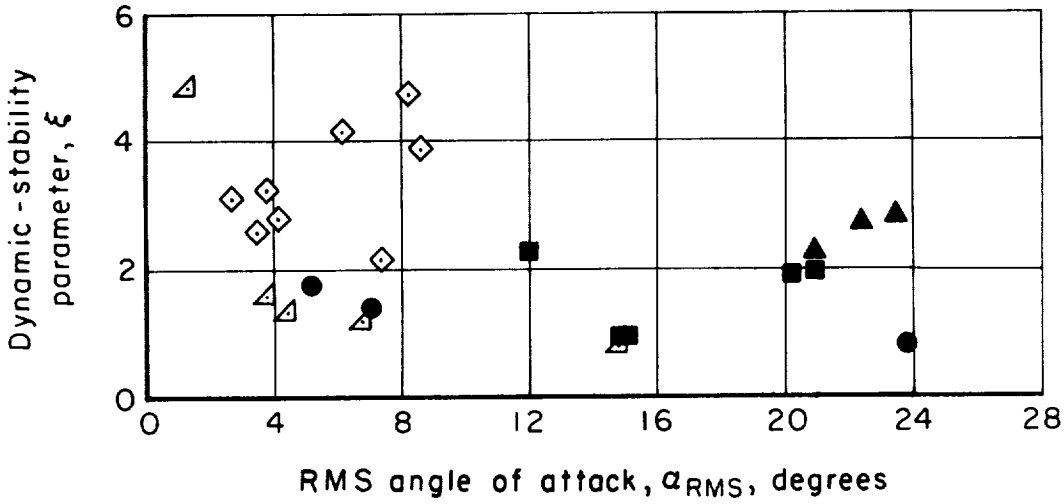

(b) Dynamic stability.

Figure 6.- Effect of afterbody geometry on the aerodynamic characteristics; $\frac{d}{r_c} = 1$; $\frac{x_{cg}}{d} = 0.20$.

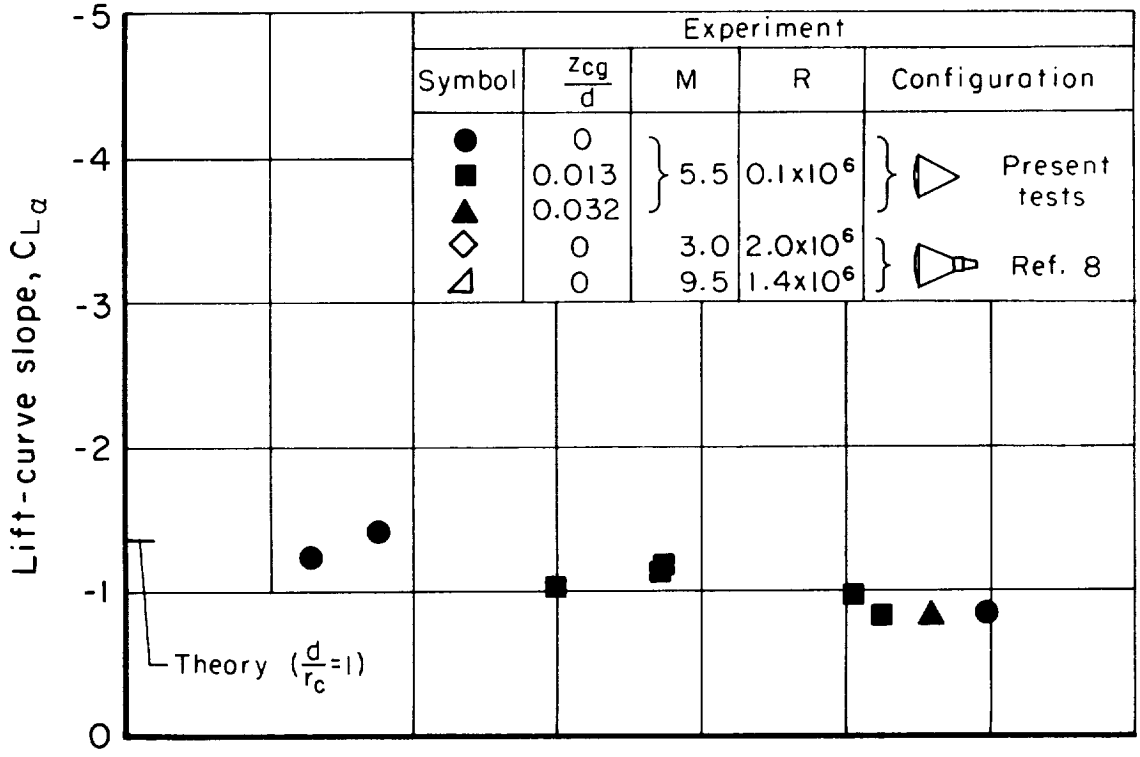

(c) Lift-curve slope.

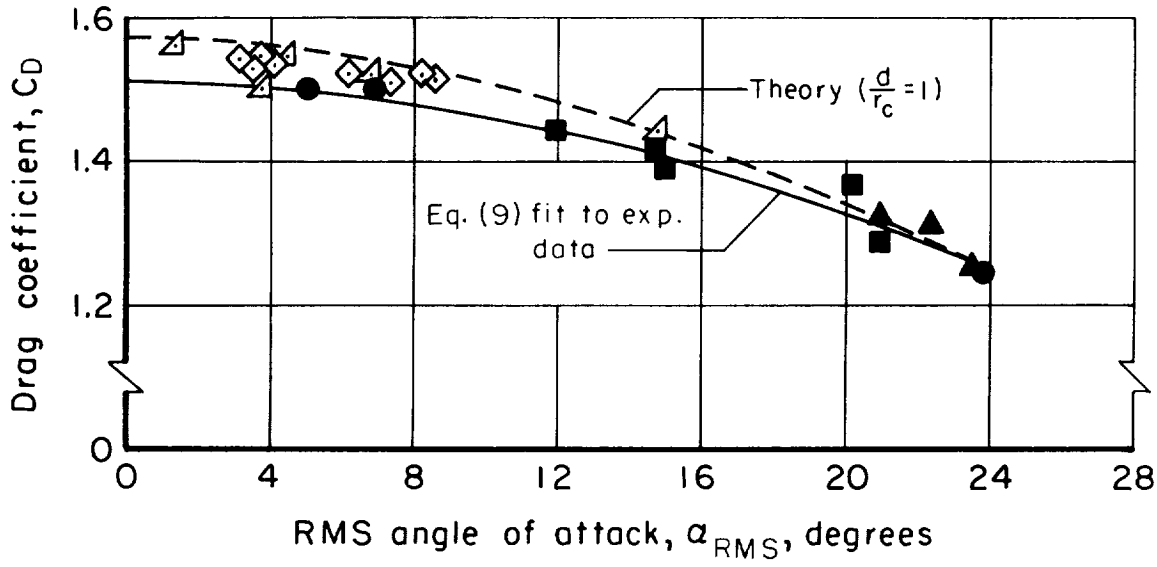

(d) Drag.

Figure 6.- Concluded.

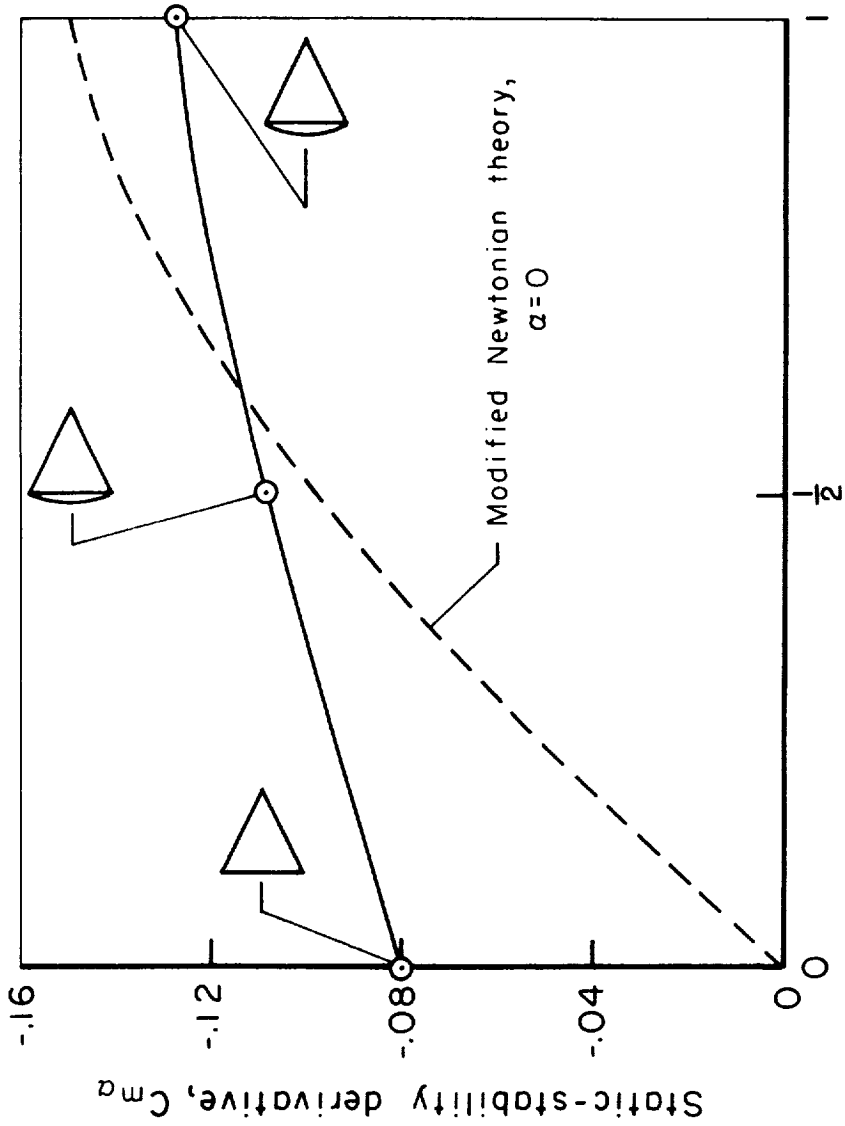

Figure 7.- Effect of front-face curvature on static stability; $\frac{x_{cg}}{d} = 0.20$.

A-7353

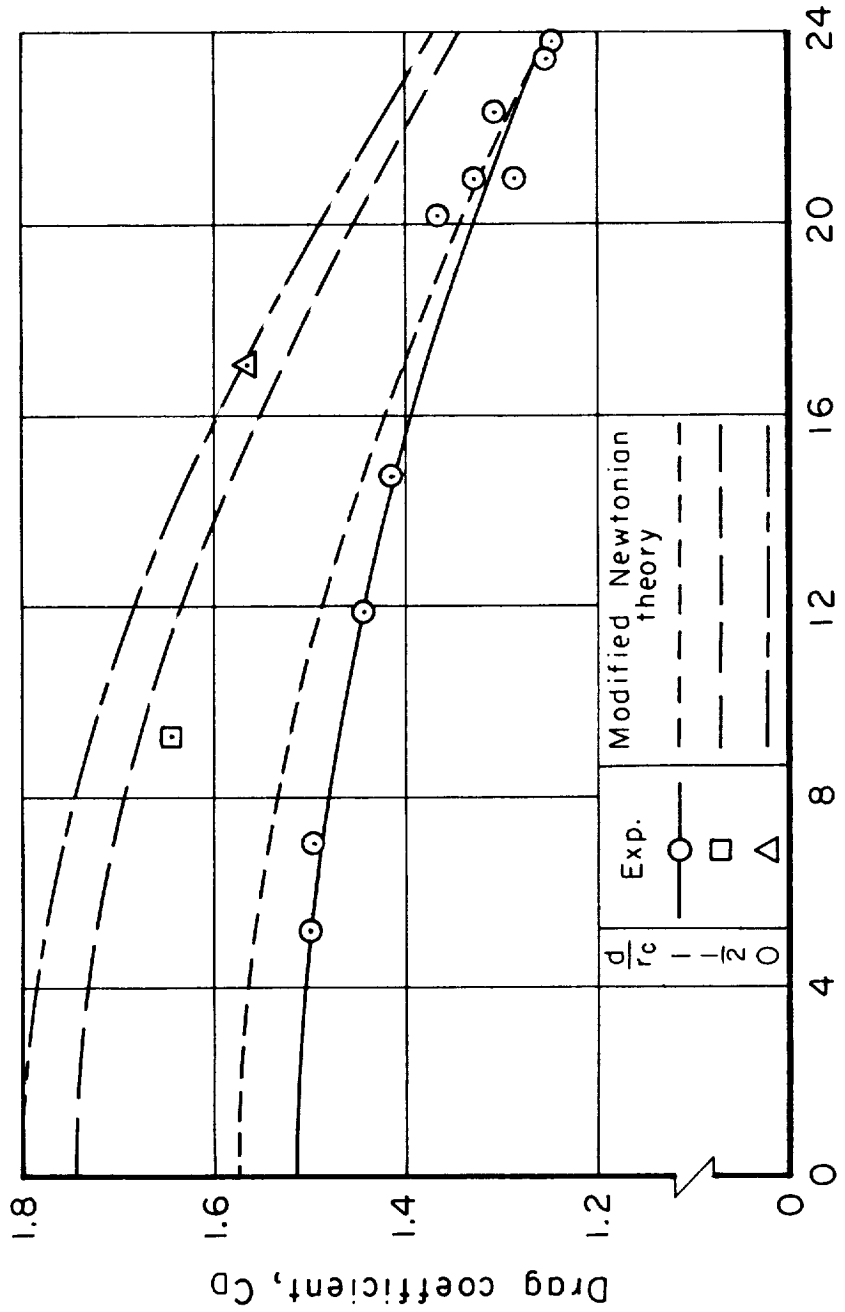

Figure 8.- Effect of front-face curvature on drag coefficient.

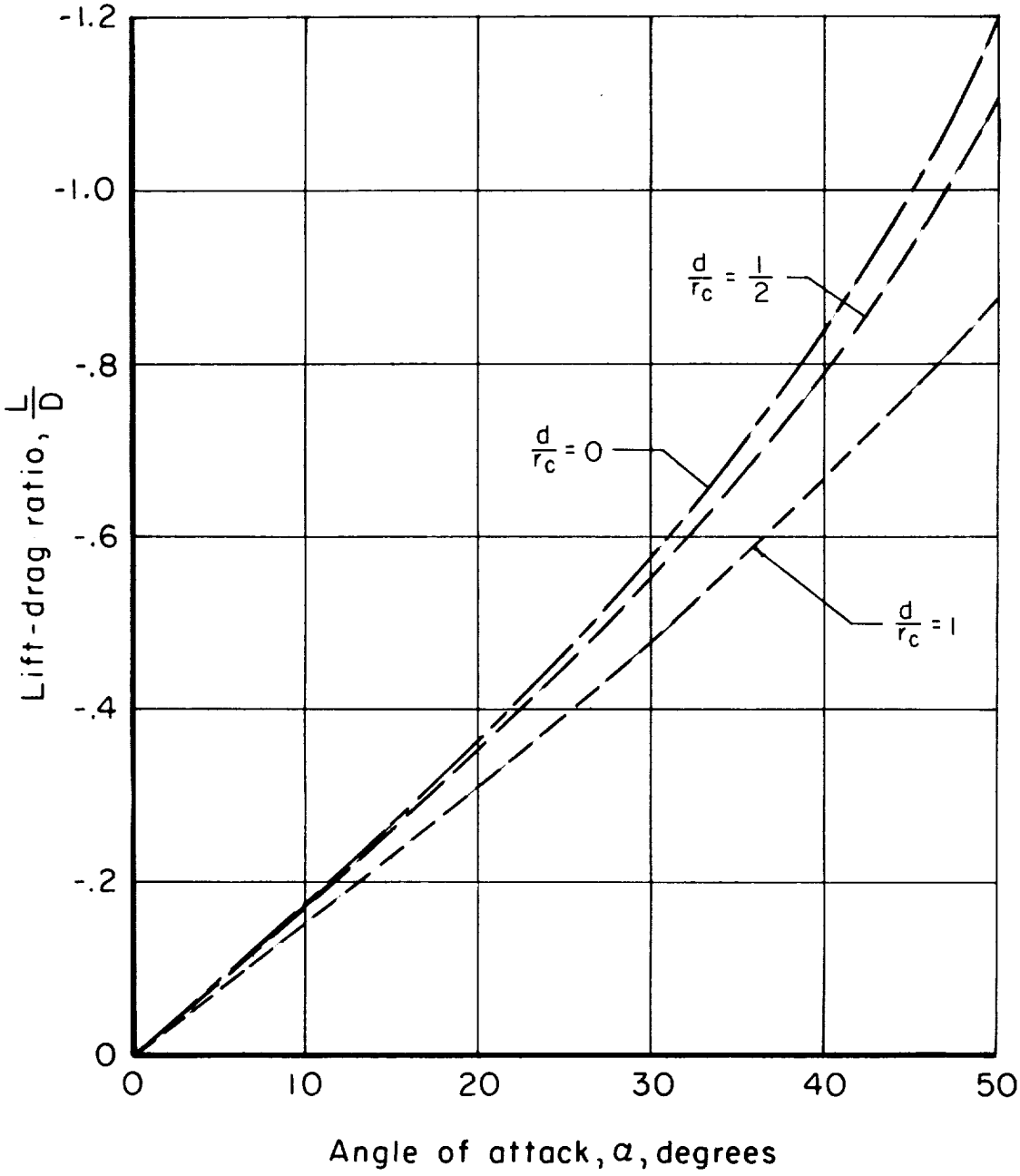

Figure 9.- Effect of front-face curvature on lift-drag ratio estimated by Newtonian theory.